Available online at www.sciencedirect.com
ScienceDirect
Catalysis Today 133–135 (2008) 129–135
CATALYSIS TODAY
www.elsevier.com/locate/cattod

Catalytic evaluation of perovskite-type oxide $LaNi_{1-x}Ru_xO_3$ in methane dry reforming

Genira Carneiro de Araujo [a,b], Sania Maria de Lima [c], José Mansur Assaf [c], Miguel Antonio Peña [b], José Luís García Fierro [b], Maria do Carmo Rangel [a,*]

[a] *Grupo de Estudos em Cinética e Catálise, Universidade Federal da Bahia, Campus Universitário de Ondina, Federação, 40 170-290 Salvador, Bahia, Brazil*
[b] *Instituto de Catálisis y Petroleoquímica, CSIC, Cantoblanco, 28049 Madrid, Spain*
[c] *Laboratório de Catálise, Departamento de Engenharia Química, Universidade Federal de São Carlos, São Paulo, Brazil*

Available online 19 February 2008

Abstract

The methane reforming with carbon dioxide (dry reforming) has been proposed as one of the most promising technologies for producing hydrogen by the use of two greenhouse gases. However, undesirable coke formation is the crucial issue to develop efficient catalysts for the reaction. In order to find alternative catalysts, which can be more resistant against coke deactivation, perovskite-type oxides $LaRu_xNi_{1-x}O_3$ ($0.0 < x < 1.0$) were studied in this work. Samples were prepared by thermal decomposition of amorphous citrate precursors followed by heating at 800 or 1000 °C, for 12 h, in air. The solids were characterized by X-ray diffraction, temperature-programmed reduction, temperature-programmed desorption, specific surface area measurements and X-ray photoelectron spectroscopy. The catalysts were reduced under hydrogen and tested in methane dry reforming at 1 atm and 750 °C. The coke produced was characterized by thermogravimetry, carbon measurement and scanning and transmission electron microscopy. The oxide precursors showed low specific surface areas and different reducing behavior. All catalysts were active in the reaction. They all produced filamentous coke but it was not harmful to the catalysts. Nickel is more active and selective to hydrogen than ruthenium but the later improved the stability of the catalysts decreasing coke formation. The most promising catalyst was the $LaNi_{0.8}Ru_{0.2}O_3$ sample, which was the most resistant against coke deposition.

Keywords: Perovskite; Dry reforming; Methane

1. Introduction

Methane reforming with carbon dioxide, also known as methane dry reforming

$$CH_{4(g)} + CO_{2(g)} \rightleftarrows 2CO_{(g)} + 2H_{2(g)}, \quad \Delta H_{298K}^{\circ} = 261\,kJ\,mol^{-1} \tag{1}$$

has attracted academic and industrial interest because of the possibility to convert two of the cheapest carbon-containing gases into valuable chemicals [1]. In addition, the dry reforming produces synthesis gas with an appropriate molar ratio for several applications such as methanol synthesis, Fischer–Tropsch reaction and acetic acid synthesis [2], besides involving a lower energy cost as compared to steam reforming. Moreover, dry reforming offers the additional advantage of consuming two greenhouse gases, transforming them into high added value products. The reaction is also more suitable for chemical energy transmission systems [1].

The properties of the dry reforming catalysts are determined by the severe conditions of operation, as illustrated by the temperatures from 500 to 800 °C. In general, catalysts are expected to show high activity and high resistance against coke deposition as well as high mechanical resistance [3]. Therefore, several catalysts have been evaluated in the target reaction in order to find solids which fit these requirements [4–7]. Most of them include catalysts based on transition metals such as nickel and noble metals like ruthenium, usually deposited over several supports [4]. The noble metal-based catalysts are less sensitive to coke deposits than the nickel-based ones. However, taking into account the high cost and the limited availability of noble metals,

* Corresponding author.
E-mail address: mcarmov@ufba.br (M. do Carmo Rangel).

0920-5861/$ – see front matter © 2008 Elsevier B.V. All rights reserved.
doi:10.1016/j.cattod.2007.12.049

nickel-based systems are the most suitable for commercial applications. These catalysts show very high activity and stability for long times of operation [3]. In spite of these advantages, they deactivate with time due to coke deposition, which have motivated the development of new nickel-based catalysts which can be more resistant against coke formation.

An attractive alternative catalyst for methane dry reforming is a perovskite-type oxide [8–10]. These oxides have the general formula ABO_3, in which the cation A of larger size is responsible for the thermal resistance of the catalyst, while the cation B of smaller size is associated with the catalytic activity. These compounds also offer the possibility to partially substitute A and B cations by other kinds of cations, thus allowing to tailor both thermal stability and catalytic performance. They are able to generate a large family of substituted oxides of general formula $A_{1-x}A'_xB_{1-x}B'_xO_3$, in which x is the substitution degree [11–15]. The extensive use of these oxides as catalysts is due not only to their ability in stabilizing unusual oxidation states of the transition metal cation (B or B′) but also to their ability in providing high oxygen mobility and also high structural stability. These characteristics make them appropriate to catalyze several reactions, mainly the redox ones [9].

In the present work, perovskite-type oxides $LaNi_{1-x}Ru_xO_3$ ($x = 0.0$, 0.1, 0.2, and 1.0) were studied with the aim of developing alternative catalysts, which can be active in the methane reforming with carbon dioxide and also can be resistant against deactivation by coke deposition.

2. Experimental

2.1. Catalyst preparation

Substituted perovskites $LaNi_{1-x}Ru_xO_3$ ($x = 0$, 0.1, 0.2, and 1) were prepared by thermal decomposition of amorphous citrate precursors [15]. A concentrated solution (10 M) of lanthanum nitrate, nickel nitrate (Merck, PA) and of ruthenium chloride (Aldrich) was prepared to obtain the La:Ni:Ru atomic ratio of $1:(1-x):x$ (where x is the partial substitution degree of the nickel). A concentrated solution (10 M) of citric acid (Aldrich) was also prepared, in such a way that the ratio of gram equivalents of citric acid and the total gram equivalents of metals of the first solution would be unity ($Eg_{acid}/Eg_{La:Ni:Ru} = 1$) to form the metallic amorphous citrate. The solutions were mixed in a glass reactor at room temperature. The resulting solution was evaporated to dryness at 70 °C under a residual vacuum of 10 Torr, to eliminate the excess of water. Products were dried at 70 °C in air for 96 h, producing the amorphous citrate precursor. It was then crushed and heated at a rate of 5 °C min^{-1} in air, at 1000 °C, except for the ruthenium-free sample which was calcined at 800 °C, for 4 h, to produce mixed oxides with perovskite structure.

2.2. Catalyst characterization

Elemental chemical composition of the samples was determined by total reflection X-ray fluorescence (TXRF). The sample (0.01 g) was ground in a mortar and then in a vibrating micropulverizer and homogenized. The analyzes were carried out in a Seifert Extra-II X-ray equipment.

The specific surface areas of the solids were measured using a Micromeritics model ASAP-2000 apparatus and the BET method. The sample (0.20 g) was previously degassed at residual vacuum of 5×10^{-3} mbar for 2 h, at 350 °C. The measurements were performed with a mixture 30% N_2/He, at 77 K. The same equipment was used to carry out the temperature-programmed reduction (TPR) analyzes. The reduction profiles were obtained by passing a 10% H_2/Ar gas mixture flow at a rate of 50 mL min^{-1} through the sample (about 0.03 g). The temperature was increased from 30 to 1000 °C at a rate of 10 °C min^{-1} and the hydrogen consumption was monitored as a function of temperature.

The temperature-programmed desorption of oxygen (TPD-O_2) analysis were performed using a Balzers QMS 200 mass analyzer on line with a microreactor. The catalyst (ca. 0.03 g) was placed into a quartz microreactor and heated at a rate of 10 °C min^{-1} in a 20% O_2/Ar flow (100 mL min^{-1}) up to 800 °C and kept at this temperature for 1 h. The solid was then cooled at room temperature, under the same flow mixture. The sample was heated again at 950 °C under argon flow (100 mL min^{-1}) and the desorbed gas was monitored by mass signal m/z of 32.

Photoelectron spectra (XPS) were obtained in a VG Escalab 200R spectrometer using a hemispherical electron analyzer and Mg Kα X-ray source. The powder samples were pressed in a copper holder, which was introduced in the pretreatment chamber, where the sample was degassed to 350 °C for 1 h, before being introduced in the analysis chamber. Peak intensities were estimated by calculating the integral of each peak after smoothing and subtraction of an S-shaped background and fitting the experimental peak by a least-squares routine using Gaussian and Lorentzian lines. Atomic ratios were computed from the intensity ratios normalized by atomic sensitivity factors. The binding energy (BE) reference was taken at the C 1s peak from carbon contamination of the samples at 284.9 eV, which gives a precision of ±0.2 eV.

The used catalysts were analyzed by thermogravimetry (TG) with the objective to identify and quantify the coke produced on the catalyst surface during the reaction. In the experiments, a TA-Instruments model SDT 2960 Simultaneous DSC-TGA equipment was used. The samples were heated at a rate of 10 °C min^{-1} in airflow from the room temperature up to 900 °C. The morphology of coke was studied by scanning and transmission electron microscopy. SEM experiments were performed with a JEOL model T330A equipment coupled to a Noran model EDS detector, while transmission analyzes were carried out using a Zeiss CTEM 902 microscopy with an energy filter Castaing–Henry. The amount of carbon on spent catalysts was determined in a Leco model CS-200 equipment, using Lecocel and the iron chip accelerator.

2.3. Catalytic activity

The catalyst performance in methane dry reforming was evaluated in a fixed bed quartz tubular microreactor, containing

0.1 g of sample. The experiments were carried out at 750 °C, under atmospheric pressure with a feed composition of CH_4:CO_2 = 1:1 and a total flow of 120 mL min^{-1}, with a continuous feed of the pre-heated reactants. Each experiment took about 10 h. To produce the active catalyst, samples were previously reduced *in situ* under hydrogen flow (40 mL min^{-1}). $LaNiO_3$ sample was activated at 750 °C for 3 h, while $LaRu_{0.1}Ni_{0.9}O_3$ and $LaRu_{0.2}Ni_{0.8}O_3$ were activated at 800 °C for 3 h and $LaRuO_3$ was activated at 800 °C, for 6 h. In all cases, a heat rate of 5 °C min^{-1} was used. The gaseous effluents were analyzed on line using a Varian model GC-380 gas chromatograph, equipped with two detectors and a Porapaq N and a Molecular Sieve 13X packed columns. The conversion of the reactants was defined as the converted amount of methane and carbon dioxide per total amount of the reactants in the reactor feed, respectively, as shown in the following equations:

$$X_{CH_4} = \frac{F_{CH_4,0} - F_{CH_4}}{F_{CH_4,0}} \quad (2)$$

$$X_{CO_2} = \frac{F_{CO_2,0} - F_{CO_2}}{F_{CO_2,0}} \quad (3)$$

where $F_{CH_4,0}$ is the inlet molar flow rates of methane (mol/s), F_{CH_4} the outlet molar flow rates of methane (mol/s), $F_{CO_2,0}$ the inlet molar flow rates of carbon dioxide (mol/s), and F_{CO_2} is the outlet molar flow rates of carbon dioxide (mol/s).

3. Results and discussion

The X-ray diffraction profiles of the samples are displayed in Fig. 1. The presence of the perovskite-type structure was confirmed for the non-substituted nickel sample, $LaNiO_3$ [10].

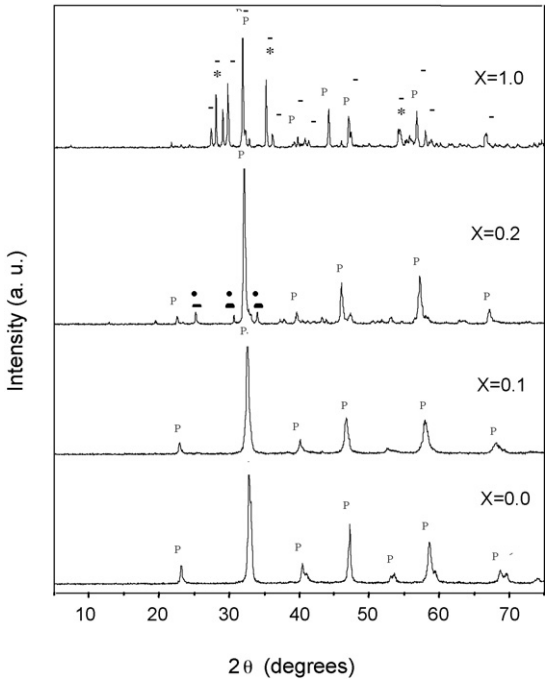

Fig. 1. X-ray diffraction patterns of $LaNi_{1-x}Ru_xO_3$ oxides: (●) LaOCl, (*) RuO_2, (P) perovskite phase and (-) $La_{3.5}Ru_{4.0}O_3$.

However, the partial substitution of nickel by ruthenium gave rise to a new phase which corresponds to the lanthanum oxychloride [16], besides the perovskite phase. In addition, when nickel was totally replaced by ruthenium, two other phases also appeared (RuO_2 and $La_{3.5}Ru_{4.0}O_3$) [17,18], instead of the desired phase ($LaRuO_3$) [19].

Table 1 compiles the atomic ratios for nickel and ruthenium relative to lanthanum, obtained from TXRF and XPS. One can see that the elemental composition of solids, got by TXRF, was not close to the theoretical one, indicating that ruthenium was not totally incorporated into the precursor and some loss occurred. This suggests that the experimental conditions were favorable to the formation of ruthenium oxide volatile compounds, which were sublimated during the heating steps. This can be explained by the high preference of ruthenium for 4+ oxidation state [14]. From the XPS results of the partially substituted nickel samples ($LaNi_{0.9}Ru_{0.1}O_3$ and $LaNi_{0.8}Ru_{0.2}O_3$), one can observe that the Ni/La and Ru/La ratios were lower than those obtained by TXRF, indicating that nickel and ruthenium migrated from the surface to the bulk of the solid. An inverse behavior was noted for the samples containing only ruthenium or nickel ($LaNiO_3$ and $La_{3.5}Ru_{4.0}O_3$), in which an enrichment of these metals was observed on the surface.

The specific surface areas of the materials were low (Table 2), which is characteristic of perovskite-type oxide [11]. The partial substitution of nickel by ruthenium did not cause a significant change in this parameter. On the other hand, the ruthenium-containing samples ($La_{3.5}Ru_{4\cdot0}O_3$) showed the lowest specific surface area.

Fig. 2 displays the reduction profiles of the samples. The $LaNiO_3$ sample showed a peak at 325 °C, assigned to the reduction of the Ni^{3+} to Ni^{2+} species, and another one at 455 °C due to the reduction of Ni^{2+} species to metallic nickel [20]. When nickel was partially substituted by ruthenium, the reduction peaks were shifted to higher temperatures, indicating that ruthenium makes nickel reduction more difficult in the

Table 1
Composition of the bulk and of the surface of $LaNi_{1-x}Ru_xO_3$ oxides

Sample	Elemental composition (TXRF)		Surface composition (XPS)	
	Ni/La	Ru/La	Ni/La	Ru/La
$LaNiO_3$	0.88	–	0.92	–
$LaNi_{0.9}Ru_{0.1}O_3$	0.81	0.09	0.66	0.040
$LaNi_{0.8}Ru_{0.2}O_3$	0.77	0.18	0.47	0.063
$La_{3.5}Ru_{4.0}O_3$	–	0.86	–	1.21

Table 2
Specific surface areas of $LaNi_{1-x}Ru_xO_3$ oxides

Sample	S_{BET} (m^2/g)
$LaNiO_3$	0.21
$LaNi_{0.9}Ru_{0.1}O_3$	1.9
$LaNi_{0.8}Ru_{0.2}O_3$	1.9
$La_{3.5}Ru_{4.0}O_3$	1.2

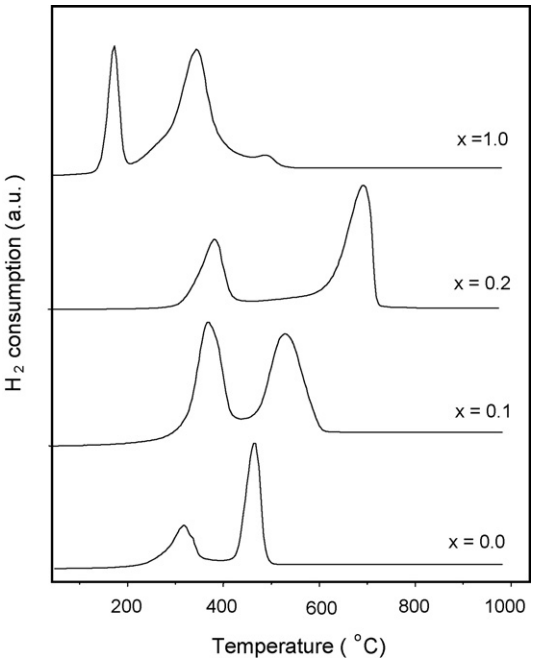

Fig. 2. Reduction profiles of $LaNi_{1-x}Ru_xO_3$ oxides.

perovskite structure. Therefore, the partially substituted samples ($x = 0.1$ and 0.2) showed the first peak centered near to 380 °C and the second one at temperatures higher than 500 °C. Hurst et al. [21] suggested that for ruthenium and nickel on different supports, the first peak is due to the reduction of the Ru^{3+} to Ru^{2+} species and/or the reduction of Ni^{3+} to Ni^{2+} species, while the second one is assigned to the reduction of the Ru^{2+} to Ru^0 species and/or reduction of Ni^{2+} to Ni^0 species. These results show that there was a synergetic effect between nickel and ruthenium that increased the resistance of both metals in the perovskite structure. The ruthenium-based perovskite was the less stable sample, whose decomposition began at about 300 °C. The ruthenium-based sample ($La_{3.5}Ru_{4.0}O_3$) displayed a third peak, at about 500 °C, which corresponds to metallic ruthenium formation, probably related to RuO_2 phase.

The binding energies (BE) of La $3d_{5/2}$, Ni 2p, Ru $3p_{3/2}$, Ru $3d_{5/2}$ and O 1s core-levels of the samples are compiled in Table 3. All sample showed binding energies typical of Ni^{3+} and Ru^{3+} and Ru^{4+} species [22], indicating that the substitution of nickel by ruthenium in the perovskite structure did not affect the electronic state of the metals. The O 1s line profile was broad in all cases and can be decomposed into three components, each one arising from an oxygen species [23]. A component at low binding energy (529.1–529.3 eV) was assigned to lattice oxygen (O^{2-}) and the intermediate component at a binding energy between 531.2 and 531.6 eV is usually ascribed to hydroxyl and/or carbonates species. The presence of carbonates was confirmed by a C 1s component around 289.1 eV, although the hydroxyl groups might be also present. The third component placed at binding energies around 533.0 eV, which disappeared upon heating the samples at 473 K, was assigned to molecularly adsorbed water molecules [24].

Table 3
Binding energies (eV) of core-levels of $LaNi_{1-x}Ru_xO_3$ oxides

Sample	Ni $2p_{1/2}$	Ru $3p_{3/2}$	Ru $3d_{5/2}$	O 1s[a]
$LaNiO_3$	873.5	–	–	529.2 (37) 531.4 (37) 533.0 (26)
$LaNi_{0.9}Ru_{0.1}O_3$	873.0	464.3	–	529.1 (36) 530.9 (26) 532.2 (33) 533.7 (5)
$LaNi_{0.8}Ru_{0.2}O_3$	873.1	464.2	283.0	529.2 (25) 530.7 (28) 532.1 (34) 533.6 (13)
$La_{3.5}Ru_{4.0}O_3$	–	464.1	282.5	529.7 (48) 531.2 (38) 532.6 (15)

[a] Peak percentages are given in parentheses.

Fig. 3 displays the results of the oxygen desorbed during the TPD-O_2 experiments. According to previous studies [25], the TPD-O_2 profiles of perovskite-type oxides showed two-oxygen desorption peaks. The peak at low temperatures is related to adsorbed oxygen (α type), while the other one at high temperatures is due to lattice oxygen (β type). From Fig. 3, we can see that the samples displayed just one peak at high temperatures (near 650 °C) associated with β type oxygen, apparently in disagreement with the XPS results. This discrepancy probably arises from sample pretreatment used in TPD experiments. The pretreatment in an O_2/Ar flow up to 800 °C prior to record TPD-O_2 profiles seems to remove the weakly adsorbed oxygen species. On looking at the desorption peak at high temperature, it can be seen that substitution of nickel by ruthenium ($x = 0.1$ and 0.2) results in a shift of the peak towards higher temperatures and also in a decrease in intensity with a concomitant broadening. This finding suggests,

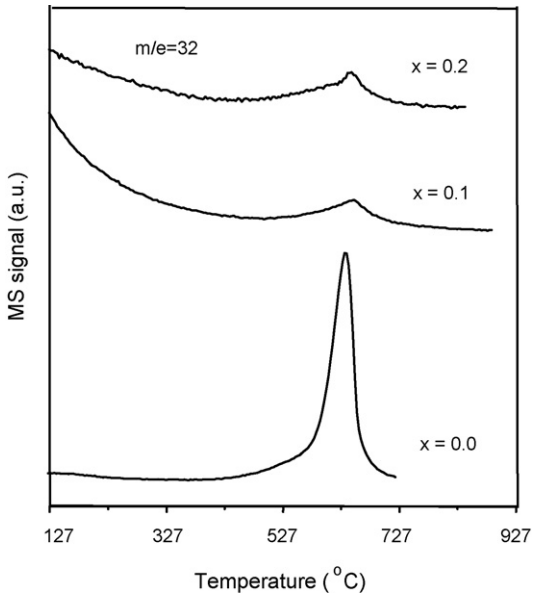

Fig. 3. TPD-O_2 profiles of $LaNi_{1-x}Ru_xO_3$ oxides.

in agreement with TPR results, a stronger strength of Ru–O–La bond as compared to the Ni–O–La one [26].

The catalytic activity results, expressed as methane and carbon dioxide conversion (Figs. 4 and 5), show that all catalysts were active in methane dry reforming but they showed different performances. It can be seen that the nickel-based sample ($LaNiO_3$) was highly active and stable. On the other hand, when the partially substituted catalysts were activated under the same conditions (750 °C, 3 h) no activity was observed. However, increasing the activation temperature up to 800 °C, the catalysts became active and the conversion increased more than 50% during the first 4 h of reaction and reached stable values after this period. This fast increase in the conversion indicates that the active sites were developed during reaction but not during activation under hydrogen prior to the reaction. In accordance with a previous work [1], the higher catalytic activity of the substituted perovskites can occur by the carbon dioxide adsorption on lanthanum oxide and by methane activation on the metallic nickel. In our work, it seems that methane and carbon dioxide are essential to produce the active phase of the substitute perovskite, probably due to the strong interaction between nickel and ruthenium, as observed in TPR profiles. In $LaNiO_3$ and $La_{3.5}Ru_{0.4}O_3$ samples, the active phase could be formed more easily since there was no interaction between the metals. Comparing the methane conversion curves as a function of time of the substituted perovskites, one can see that the Ni-richer samples showed the best performance.

The ruthenium-based catalyst, previously activated under more severe conditions (800 °C), showed high conversions since the beginning of reaction (60% of methane conversion and 70% of carbon dioxide). In this case, just a light increase of conversion was noted along reaction time.

The carbon dioxide conversions were always higher than the methane conversions as it can be inferred upon comparison of Figs. 4 and 5. This can be assigned to the occurrence of the reverse of water gas shift reaction, which also consumes carbon dioxide (Eq. (1)), simultaneously with methane dry reforming, resulting in H_2/CO ratios lower than 1.0, as shown by Fig. 6.

$$CO_2 + H_2 \rightleftarrows CO + H_2O \quad (4)$$

The thermogravimetry curves for the spent catalysts are shown in Fig. 7. The $LaNiO_3$ perovskite showed the highest amount of coke, as confirmed by carbon analysis (Table 4). On the other hand, the ruthenium-based perovskite presented a very small amount of coke. The substituted perovskites showed intermediate amounts of coke which decreased as

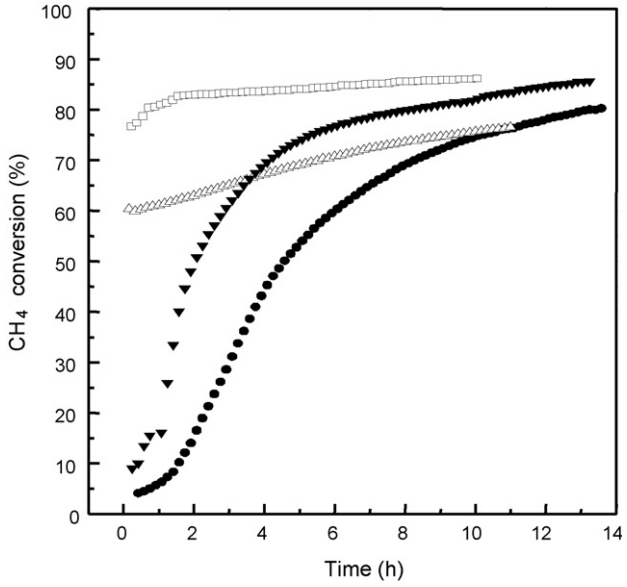

Fig. 4. Methane conversion as a function of time over the catalysts: (□) $LaNiO_3$, (▼) $LaNi_{0.9}Ru_{0.1}O_3$, (●) $LaNi_{0.8}Ru_{0.2}O_3$ and (△) $La_{3.5}Ru_{4.0}O_3$.

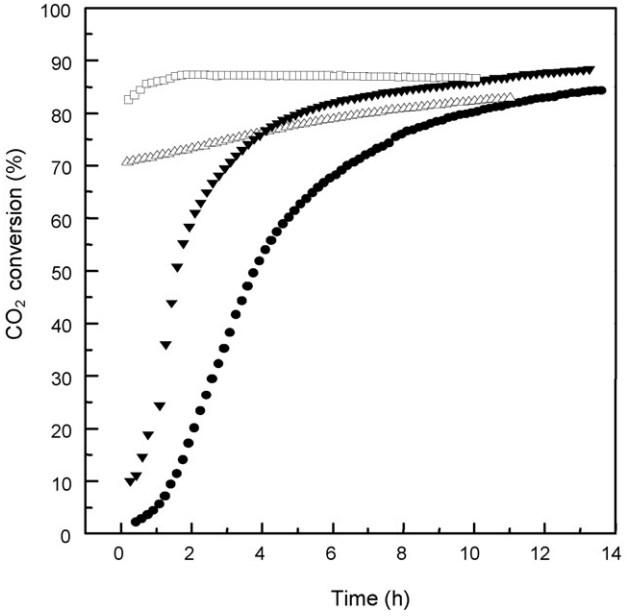

Fig. 5. Carbon dioxide yield as a function of time over the catalysts: (□) $LaNiO_3$, (▼) $LaNi_{0.9}Ru_{0.1}O_3$, (●) $LaNi_{0.8}Ru_{0.2}O_3$ and (△) $La_{3.5}Ru_{4.0}O_3$.

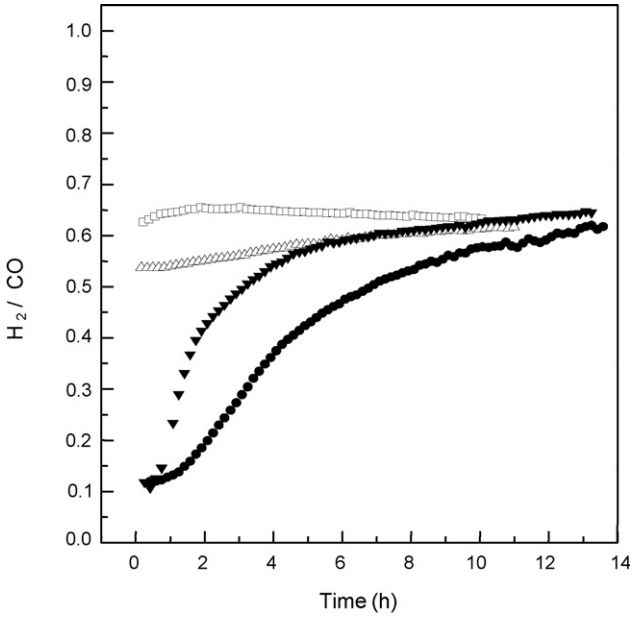

Fig. 6. Hydrogen to carbon monoxide molar ratio produced over the catalysts $LaNi_{1-x}Ru_xO_3$ oxides.

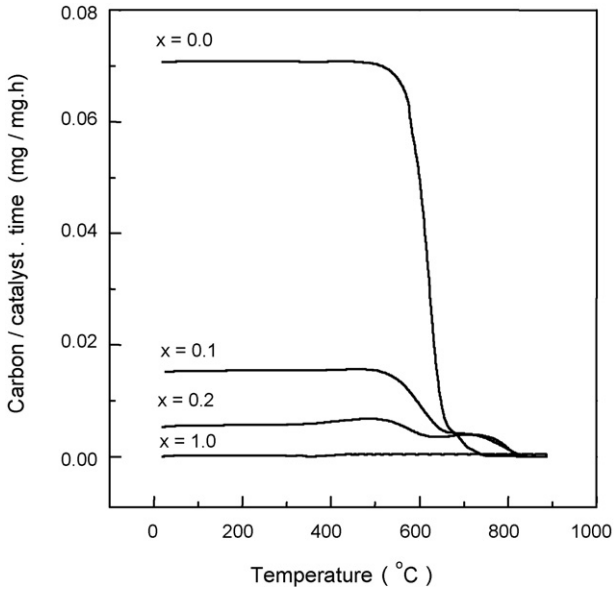

Fig. 7. Thermogravimetric curves of the catalysts, after the catalytic tests in the methane dry reforming.

Table 4
Amount of coke deposited on the spent catalysts

Sample	*C* (%)
$LaNiO_3$	65.7
$LaNi_{0.9}Ru_{0.1}O_3$	20.3
$LaNi_{0.8}Ru_{0.2}O_3$	6.86
$La_{3.5}Ru_{4.0}O_3$	0.938

the concentration of ruthenium in samples increased, as displayed in Fig. 7 and Table 4.

From Fig. 7, we can also see that the $LaNiO_3$ sample lost weight in a narrow range of temperature (around 600 °C), indicating that all deposited carbon has the same interaction with the catalyst and thus only one type of coke was produced. Since there was no decrease in activity, this carbon is supposed to be of the filamentous-type and not of encapsulating-type which would cause a decrease in activity [25]. The production of the filamentous carbon on the catalysts was confirmed by scanning electron microscopy, as illustrated in Fig. 8a. On the

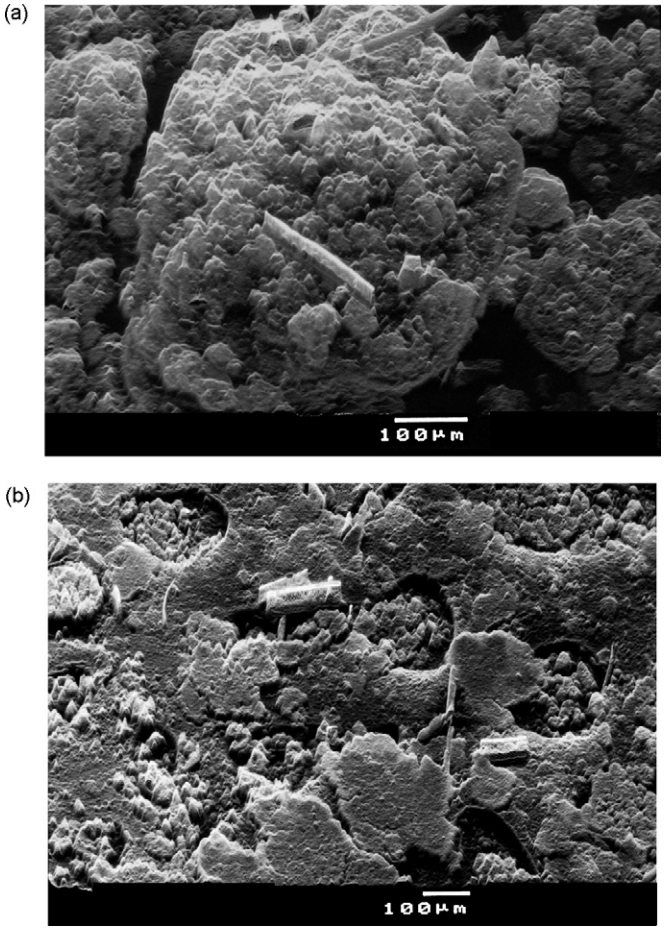

Fig. 8. Scanning electron micrographs of the catalysts after methane dry reforming: (a) $LaNiO_3$ and (b) $LaNi_{0.8}Ru_{0.2}O_3$.

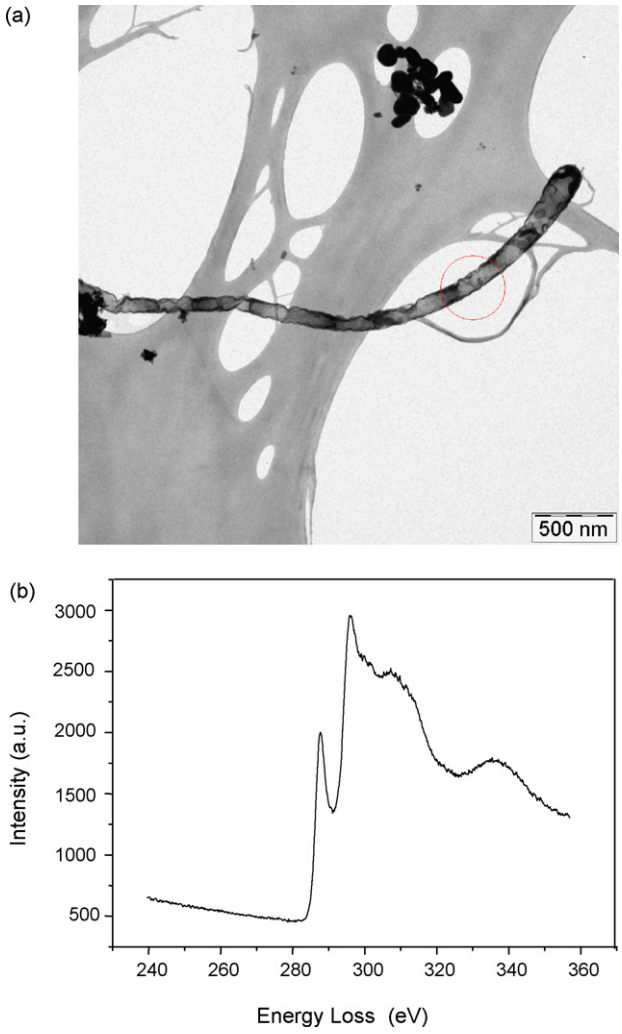

Fig. 9. (a) Transmission electron micrograph of the $LaNi_{0.8}Ru_{0.2}O_3$ sample after dry reforming and (b) EDS spectrum of the spent catalyst in the region labeled in (a).

other hand, the partially substituted catalysts showed two weight losses (600 °C and 790 °C), suggesting that two different carbon phases were produced. Fig. 8b illustrates the coke deposited on the $LaNi_{0.8}Ru_{0.2}O_3$ sample.

The filamentous carbon deposited on the samples was also studied by TEM, as illustrated in Fig. 9a, which shows a typical morphology of the filament, while Fig. 9b confirmed its carbonaceous nature. As we can see, the filamentous carbon produced has about 100–160 nm in diameter, in accordance with a previous work [27], in which filamentous carbon with 50–200 nm in diameter was produced over niobia-supported nickel and nickel–copper catalysts. These carbon filaments 30–200 nm in width consist typically of graphene layers oriented in certain manner relative to the axis (angle α) forming ''herring-bone '' ($\alpha \approx 15$–45°), ''platet'' ($\alpha \approx 90^\circ$) or multiwall carbon nanotubes (MWNT) ($\alpha \approx 0^\circ$) [28–30]. Other researchers also observed the formation of filamentous carbon with such structures over both iron and nickel-based catalysts [31,32]. It is well known [33–35] that the size of the catalytically synthesized filamentous carbon depends on the synthetic conditions and that these deposits occur preferentially on metal particles of larger size. Also, a minimum metal particle diameter (around 6 nm) is required to form filamentous carbon [35]. From Fig. 8, we can see that there was a few amounts of filamentous carbon suggesting that just some particles were big enough to produce these structures.

In all the cases, as it can be inferred from Figs. 4 and 5, the catalysts were stable during the reaction and the coke produced was not harmful to the catalyst.

4. Conclusions

The experimental conditions for synthesizing the samples of this work favored the production of perovskite-type oxides ($LaNi_{1-x}Ru_xO_3$, where $x = 0.0$, 0.1, 0.2, and 1.0), which are precursors to active catalysts in the methane dry reforming. The samples showed low specific surface areas, typical of perovskites. The partial replacement of nickel by ruthenium in the perovskite structure made the metal reduction more difficult due to a stronger strength of Ru–O–La bond as compared to the Ni–O–La one.

All the samples showed high catalytic activity in methane dry reforming and produced a hydrogen-to-carbon monoxide molar ratio of around 0.6. The nickel-based catalyst produced a large amount of coke which decreased when ruthenium was present. However, the coke produced was filamentous and was not harmful to the catalysts. The most promising catalyst was the partially substituted perovskite $LaNi_{0.8}Ru_{0.2}O_3$ which, in spite of being less active than the other samples, showed the highest resistance against carbon deposition.

Acknowledgements

This work was partly supported by CNPq (Brazil), FINEP (Brazil), MCYT (Spain) (Project MAT2001-2215-C03-01) and EU (Project ENK-2002-00682). GCA and SML gratefully acknowledge fellowship granted by CNPq and CAPES (Brazil). The authors also acknowledge Miguel Azcona and Márcia Ramos for the help in SEM analysis and Dr. C. Leite for the help in TEM analysis.

References

[1] J.T. Richardson, S.A. Paripatyadar, Appl. Catal. 61 (1990) 293.
[2] M.M.V.M. Souza, D.A.G. Aranda, M. Schmal, J. Catal. 204 (2001) 498.
[3] M.E.S. Hergart, A.M. O'Cannora, J.R.H. Ross, Catal. Today 42 (1998) 225.
[4] J.R. Rostrup-Nielsen, Steam Reforming Catalyst, Teknisk Forlag, Denmark, 1975.
[5] M.V. Twigg, Catalyst Handbook, Manson Publishing Ltd., London, 1994, p. 283.
[6] G.F. Froment, J. Mol. Catal. A: Chem. 163 (2000) 147.
[7] J.R. Rostrup-Nielsen, Stud. Surf. Sci. Catal. 81 (1994) 25.
[8] J. Barbero, M.A. Peña, J.M. Campos-Martin, J.L.G. Fierro, P.L. Arias, Catal. Lett. 87 (2003) 211.
[9] H. Falcón, J.A. Barbero, G. Araujo, M.T. Casais, M.J. Martinez-Lope, J.A. Alonso, J.L.G. Fierro, Appl. Catal. B: Environ. 53 (2004) 37.
[10] H. Falcón, J.A. Barbero, J.A. Alonso, M.J. Martinez-Lope, J.L.G. Fierro, Chem. Mater. 14 (2002) 2325.
[11] M.A. Peña, J.L.G. Fierro, Chem. Rev. 101 (2001) 1981.
[12] A. Peña, J. Gutierrez, L.M. Rodriguez-Martinez, J.M.T. Barandiaran, T. Hernandez, T. Rojo, J. Magn. Magn. Mater. 254 (2003) 586.
[13] S. Nakamura, M. Tanaka, H. Kato, Y. Tokura, J. Phys. Soc. Jpn. 72 (2003) 424.
[14] N.K. Labhsetwar, A. Watanabe, T. Mitsuhashi, Appl. Catal. B: Environ. 40 (2003) 21.
[15] J.M.D. Tascon, S. Mendioroz, L.G. Tejuca, Z. Phys. Chem. NF 124 (1981) 109.
[16] JCPDS-ICDD, 34-1494 card index.
[17] JCPDS-ICDD, 71-2273 card index.
[18] JCPDS-ICDD, 71-1929 card index.
[19] JCPDS-ICDD, 82-1477 card index.
[20] L. Cao, Y. Chen, W. Li, in: M. De Pontes, R.I. Espinoza, C.P. Nicolaides, J.H. Scholz, M.S. Scurrell (Eds.), Natural Gas Conversion IV, Elsevier, Amsterdam, 1997, p. 467.
[21] N.W. Hurst, S.J. Gentry, A. Jones, B.D. McNicol, Catal. Rev. Sci. Eng. 24 (1982) 233.
[22] M. Crespin, W.K. Hall, J. Catal. 69 (1981) 359.
[23] L.G. Tejuca, J.L.G. Fierro, J.M.D. Tascon, Adv. Catal. 36 (1989) 237.
[24] N. Yamazoe, Y. Teraoka, T. Seiyama, Chem. Lett. 1767 (1981).
[25] D.L. Trimm, Catal. Today 49 (1999) 3.
[26] T. Seiyama, N. Yamazoe, K. Eguchi, Ind. Eng. Chem., Prod. Res. Dev. 24 (1985) 19.
[27] J. Li, G. Lu, K. Li, W. Wangm, J. Mol. Catal. A: Chem. 221 (2004) 105.
[28] L.B. Avdeeva, T.V. Reshetenko, V.B. Fenelonov, A.L. Chuvilin, Z.R. Ismagilov, Carbon 42 (2004) 2501.
[29] L.B. Avdeeva, T.V. Reshetenko, Z.R. Ismagilov, V.A. Likholobov, Appl. Catal. A: Gen. 228 (2002) 53.
[30] T.V. Reshetenko, L.B. Avdeeva, Z.R. Ismagilov, V.V. Pushkarev, S.V. Cherepanova, A.L. Chuvilin, Carbon 41 (2003) 1605.
[31] C.D. Tan, R.T.K. Baker, Catal. Today 63 (2000) 3.
[32] J. Zhang, A. Schneider, G. Inden, Corros. Sci. 45 (2003) 1329.
[33] S.G. Zavarukhin, G.G. Kuvshinov, Chem. Eng. J. 120 (2006) 139.
[34] M.C. Demicheli, D. Duprez, J. Barbier, E.N. Ponzi, O.A. Ferretti, J. Catal. 145 (1994) 437.
[35] D. Duprez, M.C. Demicheli, P. Marecot, J. Barbier, O.A. Ferretti, E.N. Ponzi, J. Catal. 124 (1990) 324.